ORIGINAL ARTICLE

Experimental investigation of hydrogen-intensified synthetic natural gas production via biomass gasification: a technical comparison of different production pathways

Alexander Bartik[1] · Florian Benedikt[1] · Josef Fuchs[1] · Hermann Hofbauer[1] · Stefan Müller[1]

Abstract

A sustainable and secure energy supply requires alternative concepts for energy generation. Utilizing biomass to produce synthetic natural gas (SNG) allows the synthesis of a currently widely used energy carrier on a renewable basis. The additional integration of hydrogen increases the carbon utilization of the biomass. This study experimentally investigates and compares the production of raw-SNG in three novel process chain configurations combining the advanced dual fluidized bed (DFB) gasification technology, gas cleaning units, and a fluidized bed methanation reactor. The three process chains comprise the direct methanation of DFB product gas, a hybrid route with hydrogen addition to the DFB product gas, and the methanation of a hydrogen-enriched product gas generated through DFB gasification with in situ CO_2 removal (SER process). The direct methanation of the DFB product gas yielded a raw-SNG CH_4 content of 40 vol.-%$_{db}$ at 360 °C and atmospheric pressure conditions. Through the integration of external hydrogen in a hybrid process, the carbon utilization of the biomass could be increased from 37% to around 70% at an unchanged cold gas efficiency of 58–59%. Via the SER process, a high raw-SNG CH_4 content of 70 vol.-%$_{db}$ was achieved at an increased cold gas efficiency of 66% without the need for external hydrogen. Finally, a comparison points out the main advantages of the process configurations and provides a decision basis for novel SNG production pathways.

Keywords Sustainable and renewable synthetic natural gas · Advanced dual fluidized bed steam gasification · Sorption enhanced reforming · Fluidized bed methanation · Hydrogen integration · Experimental investigation in pilot scale

Nomenclature

CR	Combustion reactor
DFB	Dual fluidized bed
FICFB	Fast internally circulating fluidized bed
GCMS	Gas chromatography linked with a mass spectrometer
GR	Gasification reactor
feed	In the feed gas to the methanation reactor
KPI	Key performance indicator
out	In the outlet of the methanation reactor
raw-SNG	Raw synthetic natural gas after methanation/before upgrading
RME	Rapeseed methyl ester
SNG	Synthetic natural gas
SER	Sorption enhanced reforming
WHSV	Weight hourly space velocity in Nl/(g$_{cat}$ h)
$\dot{n}_i$	Molar flow of species i in mol/s
N_i	Number of carbon atoms in species i
$\dot{m}_{C,CH_4,RawSNG}$	Amount of carbon in CH_4 in the raw-SNG in kg/h
$\dot{m}_{C,GR,fuel}$	Amount of carbon in the fuel to the GR in kg/h
$\dot{m}_{GR,fuel,daf}$	Amount of dry and ash-free fuel to the GR in kg/h
$\dot{m}_{H_2O,GR,fuel}$	Amount of water to the GR through the fuel in kg/h
$\dot{m}_{steam,GR}$	Amount of steam to the GR through the gasification agent in kg/h
$P_{CR,fuel}$	Chemical energy of the fuel to the CR in kW
$P_{GR,fuel}$	Chemical energy of the fuel to the GR in kW

✉ Alexander Bartik
   alexander.bartik@tuwien.ac.at

[1] Institute of Chemical, Environmental and Bioscience Engineering, TU Wien, Getreidemarkt 9/166, 1060 Vienna, Austria

P_{H_2}	Chemical energy of the external hydrogen in kW
P_{PG}	Chemical energy of the product gas in kW
P_{RawSNG}	Chemical energy of the raw-SNG in kW
$\dot{Q}_{loss,DFB}$	Heat losses of the DFB system in kW
SN	Stoichiometric number of the feed gas
U	Superficial gas velocity
U_{mf}	Minimum fluidization velocity
X_{CO}	Carbon monoxide conversion in %
X_{CO_2}	Carbon dioxide conversion in %
X_{H_2}	Hydrogen conversion in %
Y_{CH_4}	Methane yield in %
y_i	Molar fraction of species i
φ_{SF}	Steam-to-fuel ratio
$\eta_{CG,o,DFB}$	Overall cold gas efficiency of the DFB system in %
$\eta_{CG,o}$	Overall cold gas efficiency of the full process chain in %
η_C	Carbon utilization efficiency in %

1 Introduction

The replacement of fossil fuels by renewable energy carriers and the respective production pathways are crucial in mitigating climate change and securing the independence of energy imports within the European Union. Synthetic natural gas (SNG) from renewable resources, as well as biogas from fermentation, has the potential to contribute to these goals, especially considering the limited time frame to accomplish the transformation [1].

Over the last two decades, biological and catalytic SNG production technologies from renewable resources have been developed. The two main strategies for the catalytic production of SNG are as follows: (i) the utilization of biogenic feedstock via a thermochemical pathway and (ii) the utilization of renewable electricity via an electrochemical pathway together with biogenic carbon dioxide [2, 3]. Both routes have been demonstrated on a large scale, e.g., the 32 MW_{th} GoBiGas SNG plant in Gothenburg, Sweden [4] or the 6 MW_{el} Power-to-Gas plant in Werlte, Germany [5]. The latter produces SNG through the hydrogenation of biogenic carbon dioxide in a molten salt-cooled tube bundle reactor. An alkaline electrolysis provides the necessary hydrogen, and the carbon dioxide is separated through amine scrubbing from a nearby biogas plant. The GoBiGas plant, on the other hand, produces SNG through dual fluidized bed (DFB) gasification of woody biomass and consecutive gas cleaning and catalytic conversion to methane in a fixed bed reactor cascade. A generic flow sheet of such a process chain is depicted in Fig. 1a. In the DFB gasification system, the biogenic feedstock is converted to a product gas, typically
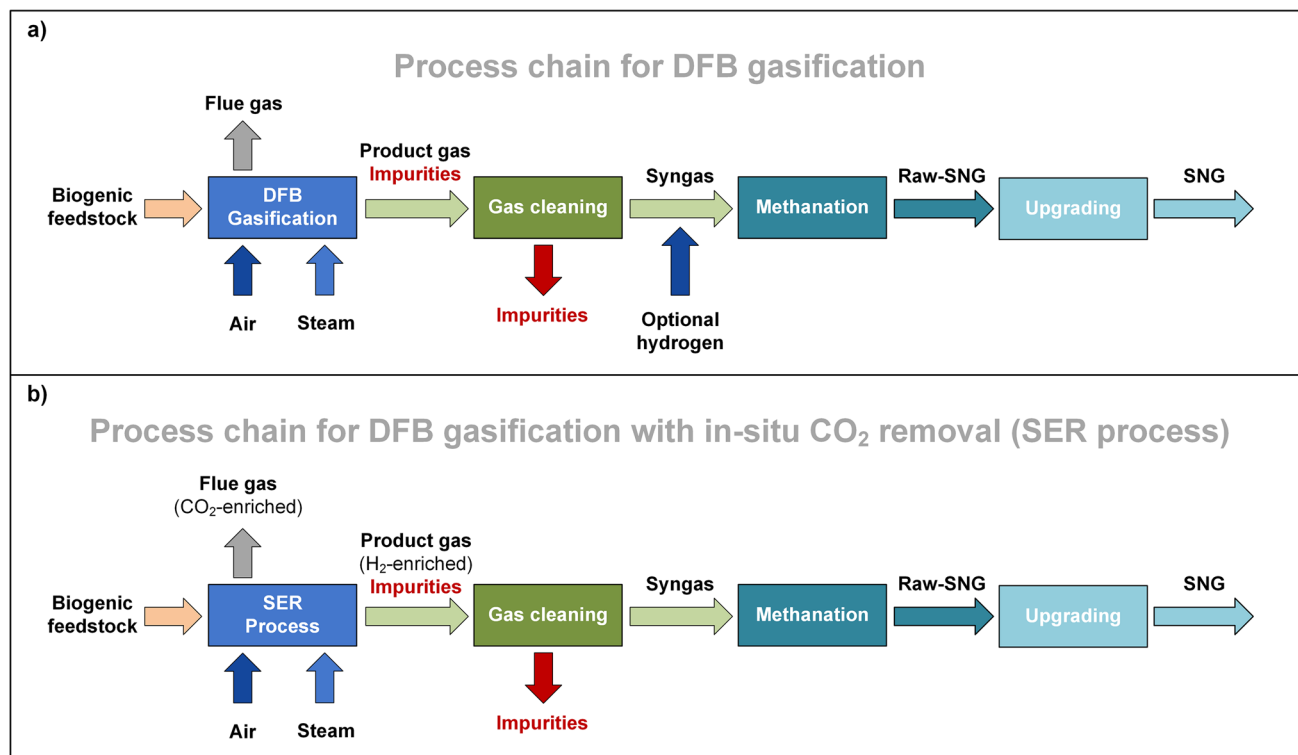

Fig. 1 Basic process layouts of two SNG production processes based on DFB gasification: **a** DFB gasification with optional hydrogen addition to the syngas, **b** DFB gasification with in-situ CO$_2$ removal (SER process)

utilizing steam as a gasification agent. Depending on the type and quality of the feedstock, a certain amount of impurities must be removed from the product gas to protect the methanation catalyst from poisoning and deactivation and achieve the necessary gas quality for the respective application. The cleaned product gas or syngas is then catalytically converted to raw-SNG in the methanation section. Depending on the applied concept, an upgrading of the raw-SNG is necessary to fulfill the national feed-in regulations of the natural gas grid. The upgrading might comprise gas drying, carbon dioxide, and hydrogen separation [6].

The necessity for carbon dioxide, or carbon separation in general, arises from the typical composition of woody biomass. On average, the elemental composition can be written as $CH_{1.44}O_{0.66}$ [7]. For the hydrogenation of the main carbon-containing species in the syngas, namely carbon monoxide and carbon dioxide, a molar ratio of three and four, respectively, is required. Due to this discrepancy, only limited utilization of biogenic carbon can be achieved. For example, the GoBiGas plant reports a carbon utilization factor of around 30% [8]. An interesting way to increase carbon utilization is the combination of the thermochemical conversion technology with power-to-gas by adding hydrogen before the methanation reactor (optional hydrogen), as indicated in Fig. 1a. This hybrid approach improves the production of SNG from a technical and ecological point of view. However, the integration of hydrogen production is generally a cost driver that influences the process' competitiveness [9, 10]. Moreover, hydrogen must not originate from fossil resources for an ecologically viable concept. Therefore, various renewable hydrogen production methods are currently under investigation. The most widely discussed and matured technology is water electrolysis [11]. However, there is a multitude of other technologies utilizing thermal, electrical, photonic, or biochemical energy to convert water or biomass to hydrogen [12]. Some examples are electrical or thermochemical water splitting [13, 14], biomass gasification [15], and dark or photo-fermentation of biogenic materials [16].

To avoid any additional hydrogen production, a modified DFB gasification process can be applied: The so-called sorption enhanced reforming (SER) process [17] allows for the in situ adaptation of the product gas composition towards high hydrogen contents via in situ CO_2 removal in the DFB gasification system (Fig. 1b). This way, the product gas composition can be matched to the requirements of the methanation section. Bartik et al. [18] and Brellochs [19] showed on a theoretical basis that potentially no CO_2 separation would be required for upgrading the raw-SNG to the gas grid requirements. Experimentally, the methanation of typical SER product gases was shown by Bartik et al. [20] in a fluidized bed reactor and by Gómez et al. [21] in two-fixed bed methanation reactors utilizing synthetically premixed gases. However, there seems to be no experimental

investigation of the whole process chain, including gasification, gas cleaning, and methanation.

The hybrid route with optional hydrogen addition (Fig. 1a) was already proposed on a theoretical basis by Gassner and Maréchal [9] in 2008. Alamia et al. [22] simulated the integration of hydrogen to an optimized GoBiGas plant and calculated cold gas efficiencies between 70 and 73% for SNG production. Some experimental investigations were carried out by Salbrechter and Schubert [23]. They performed methanation experiments in fixed-bed reactors with varying hydrogen contents in the premixed syngas. They argue that a substoichiometric hydrogen addition leads to a good trade-off between electrolysis capacity and the overall efficiency, which they calculated at 60% for a large-scale plant. However, around 17 vol.-% of CO_2 is still in the raw-SNG and needs to be separated before grid injection. Multiple alternative concepts for the integration of hydrogen in the SNG production process have been proposed. For example, Menin et al. [24] modeled a combination of biomass steam gasification, alkaline water electrolysis, and biological methanation in a trickle-bed reactor and calculated a cold gas efficiency of 50.6%. Giglio et al. [25] conceptualized a catalytic methanation process in isothermal reactors in combination with solid oxide electrolysis and oxygen/steam-blown gasification and calculated cold gas efficiencies as high as 71.7%. From an experimental point of view, Leimert et al. [26] combined the heatpipe reformer gasification technology with a polytropic fixed bed methanation reactor and demonstrated the production of raw-SNG with additional hydrogen. However, due to limitations in the methanation reactor, the residual H_2 and CO_2 concentrations in the raw-SNG were quite high. Another demonstration of a hybrid process concept was shown by Witte et al. [27]. They directly upgraded biogas in a fluidized bed methanation reactor with external hydrogen over more than 1000 h with an average methane yield of 96%. Other researchers have modeled the hydrogen addition to syngas to produce other fuels and chemicals like dimethyl ether [28] and methanol [29]. Industrial process gases are also an interesting carbon source for a further hydrogenation to methane. For example, off-gases from steelworks can be utilized for methane synthesis with additional hydrogen [30]. In the case of direct iron ore reduction with hydrogen, the off-gas already consists of a considerable amount of hydrogen, which can be utilized as the reducing agent for a consecutive methanation reaction [31]. However, for the hybrid route investigated in this study, no experimental investigations connecting DFB gasification with fluidized bed methanation and hydrogen addition seem to be available.

In this study, we investigate several novel process chains for the production of raw-SNG from woody biomass on a pilot scale. At TU Wien, a 100 kW_{th} advanced DFB pilot plant converting woody biomass to product gas is coupled

with gas cleaning units and a 10 kW$_{th}$ fluidized bed methanation reactor to produce raw-SNG. Figure 2 (left) depicts the basic principle of the DFB gasification process. In the gasification reactor (GR), the biogenic feedstock is converted to a product gas containing mainly H_2, CO, CO_2, and CH_4 with steam as a gasification agent. Due to the allothermal operation of the GR, a nearly nitrogen-free product gas is obtained. However, impurities, like tars and nitrogen- and sulfur-containing species, might need to be removed in the gas cleaning section, depending on the quality of the feedstock. The GR is coupled with a combustion reactor (CR) through a solid circulation loop. In the CR, ungasified char is combusted with air to heat up the bed material. Since the CR is operated as a fast fluidized bed, the hot bed material is transported back to the GR, where it sustains the endothermic gasification process. Via the usage of limestone as bed material and suitable temperature levels in the reactors, the in situ removal of CO_2 from the gasification reactor can be facilitated (Fig. 2 (right)). At comparably low temperatures of 600 to 700 °C in the GR, $CaCO_3$ is formed out of CaO and gaseous CO_2. The removal of gaseous CO_2 from the product gas stimulates the water–gas-shift reaction and leads to an increased hydrogen content (up to 70 vol.-%$_{db}$). The captured CO_2 is transported to the CR as $CaCO_3$ together with the bed material and char. At elevated temperatures in the CR, the $CaCO_3$ is calcined. Thus, gaseous CO_2 is released again in the CR, and CaO is formed out of $CaCO_3$. Two main parameters which allow the targeted adjustment of the product gas composition are the gasification temperature and the bed material cycle rate [17]. More information on the DFB process and the overall process chain can be found in Sect. 2 and is also reported in literature [32–34].

The aim of this work is the demonstration of raw-SNG production through advanced DFB gasification, gas cleaning, and fluidized bed methanation. The novelty lies in the investigation of multiple novel process configurations on a pilot scale regarding gas compositions, conversions, yields, and efficiencies. Furthermore, extensive analytical measurements show the whereabouts and quantities of impurities over the entire SNG process chains. The investigations include three configurations, namely

(a) DFB gasification and direct methanation of the DFB product gas (DFB-Std)

(b) DFB gasification with external hydrogen addition to the product gas and methanation of the hydrogen-enriched product gas (DFB + H_2)

(c) DFB gasification with in-situ CO_2 removal (SER process) and direct methanation of the hydrogen-enriched product gas without external hydrogen addition (SER)

Finally, a comparison of the three configurations shows the advantages and disadvantages of the respective process chains and therefore helps determine a suitable process depending on the defined goals.

2 Materials and methods

2.1 Complete process chain

Figure 3 shows a basic flowsheet of the process chain for raw-SNG production at TU Wien. The main units are

- A 100 kW$_{th}$ advanced DFB gasification reactor
- A biodiesel (rapeseed methyl ester (RME)) scrubber
- Activated carbon and zinc oxide (ZnO) adsorber beds
- And a 10 kW$_{th}$ fluidized bed methanation reactor

The left part of the diagram depicts the fuel-feeding system. Three fuel hoppers are available to feed the feedstock via screws into the lower GR. The generated product
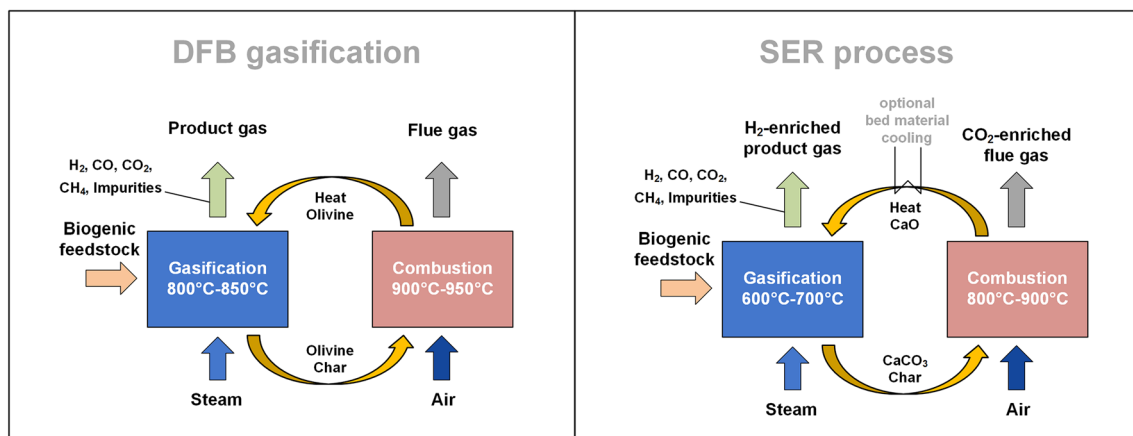

Fig. 2 Basic principle of DFB gasification (left) and DFB gasification with in situ CO_2 removal (SER process) (right)
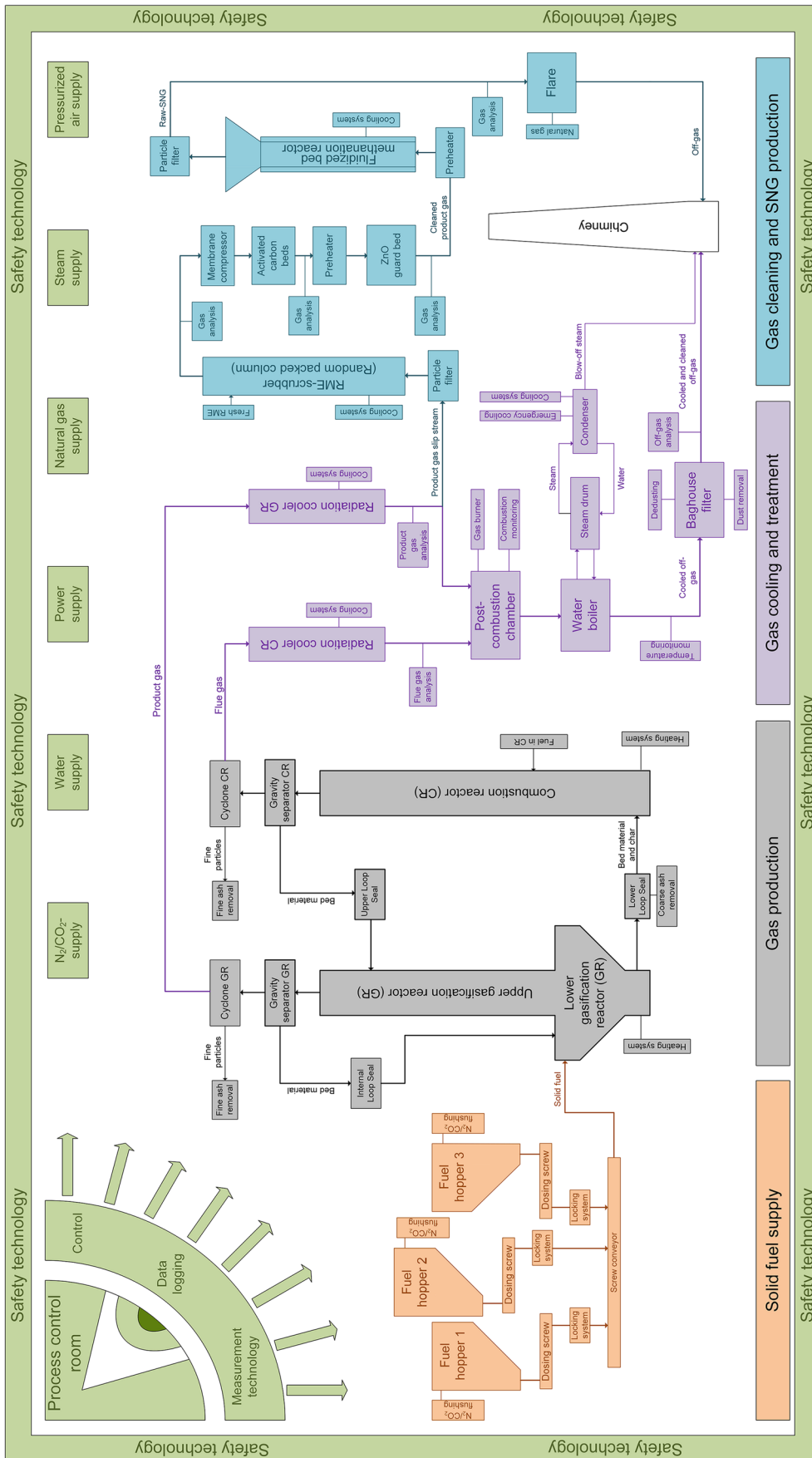
**Fig. 3** Basic flow sheet of the SNG process chain at TU Wien

gas further reacts in the upper GR and leaves the DFB system after particle separation in a gravity separator and a cyclone. After passing through a radiation cooler, a partial flow of the product gas is directed toward the SNG process chain. The unutilized part of the product gas is burnt in a post-combustion chamber together with the flue gas from the CR. Before the off-gas is vented to the atmosphere, the gas is cooled in a boiler, and dust is separated in a baghouse filter.

The partial product gas flow directed to the SNG process chain is cleaned in a filter stuffed with glass wool and enters the RME scrubber. The following membrane compressor is used as a blower to set the required volume flow for the methanation reactor. Since the process chain is operated at almost atmospheric pressure, no significant pressure increase is desired. To further remove impurities from the product gas stream, the gas passes through two activated carbon beds and a ZnO bed at elevated temperatures. The preheated gas then enters the fluidized bed methanation reactor, where the syngas is converted to raw-SNG. A glass wool filter holds back potentially carried-out catalyst particles and a natural gas–operated flare is used to burn the raw-SNG downstream of the gas analysis measurements. Auxiliary systems, like process media supply, measurement technology, a process control system, and safety measures, accompany the main process chain. In Sects. 2.2–2.4, a more detailed description of the single process units follows.

2.2 100 kWth advanced dual fluidized bed pilot plant

The advanced DFB pilot plant at TU Wien is a further development of industrially realized DFB gasification plants. Figure 4 shows pictures of the pilot plant (left) and a schematic drawing of the reactor concept (right) [33]. Here, a more detailed drawing of the constructional design of the reactor is depicted, compared to the basic principle of the DFB system in Figs. 2 and 3. The same reactor is used for DFB gasification and the SER process. Feedstock enters the lower GR through a fuel-feeding screw above the top of the bed (on-bed feeding). In the lower GR, the pyrolytic decomposition and gasification of the solid feedstock take place. The CR is designed as a fast fluidized bed, where parts of the unconverted feedstock combust together with additional fuel (fuel to CR). Both reactors are connected via loop seals, enabling bed material circulation between the reactors. The novelty of the advanced concept mainly lies in the implementation of an upper gasification reactor and gravity separators. The upper GR is designed as a counter-current column with local constrictions, which increases the gas–solid contact time and the turbulence between the bed material and the upward-flowing product gas. Gravity separators ensure a gentle gas–solid separation and allow the utilization of soft bed materials like limestone. An internal loop seal allows the recirculation of particles within the upper and lower

Fig. 4 Photos of the 100 kW$_{th}$ advanced DFB pilot plant at TU Wien (left) and schematic drawing of the reactor design (right) [33]
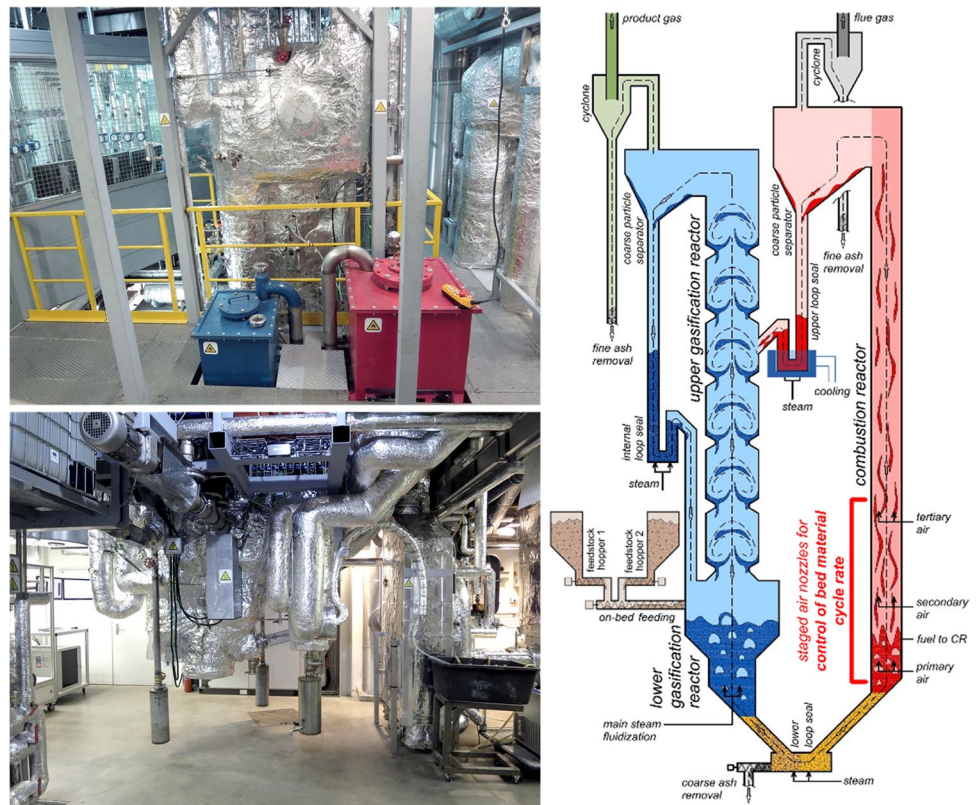
GR. To reach a suitable temperature spread between CR and GR for the SER process, a loop seal cooling is installed additionally. Furthermore, the bed material cycle rate can be influenced by staged air nozzles in the CR. By leaving the total amount of air introduced into the CR constant, but shifting the partial amounts at a specific height, an efficient control of the bed material cycle rate is possible (primary air, secondary air, tertiary air). A detailed description of the design is documented by Schmid [33]. A detailed analysis of DFB gasification and SER is not within the scope of this paper since the mechanisms of these gasification processes are well documented in the literature [17, 32, 34].

Olivine is commonly used as bed material for DFB gasification. It is a magnesium-iron-silicate-based mineral that forms a calcium-rich layer on the surface of the particles through the interaction with the fuel ash and thus promotes its catalytic activity [35]. Therefore, limestone has been extensively investigated as an alternative, catalytically highly active bed material [36]. In this investigation, a 80/20 wt.-% olivine/limestone mixture is used as bed material for the DFB gasification and pure limestone for the SER process to enable the in-situ CO_2 removal. Softwood pellets with quality class A1 according to ISO 17225–2 are used as feedstock for the test runs. Table 1 shows the results of the ultimate and proximate analysis of the softwood pellets. The pellets show low water and ash contents as well as low amounts of sulfur and chlorine and high ash melting temperatures. These high-quality pellets were used in all test runs as a reference fuel for a fair comparison of the different process configurations. The compositions of the bed materials are listed in the supplementary material.

2.3 Gas cleaning

Ni catalysts are prone to deactivation through impurities in the product gas. Thus, it is crucial to implement a sufficient gas-cleaning strategy to protect the catalyst from poisoning and coke formation. To this end, a particle filter, an RME scrubber, activated carbon beds, and a ZnO guard bed are installed (Fig. 5). The particle filter is a simple glass wool stuffed cylinder that holds back dust particles resulting from bed material attrition, fuel ash, and unconverted biomass char. The RME scrubber is designed as a randomly packed column with a diameter of 0.1 m, a demister, and a connected phase separator. In the counter-current column, tar components are condensed and dissolved in the RME. Furthermore, steam condenses and water-soluble substances like NH_3 and HCl dissolve in the water phase. In the phase separator, a division occurs into a water phase, an emulsion phase, and an RME phase. The RME phase is recirculated to the scrubber, while the water and emulsion phases are withdrawn periodically. The scrubber is designed for an operating temperature between 10 and 50 °C. A cryostat provides the necessary cooling power. Fixed-bed adsorption in two activated carbon beds is performed to reduce tar components that have not been separated in the scrubber and to adsorb sulfur compounds. A Desorex K 43 and an Oxorbon K40 J from Donau Carbon are used for this purpose. A ZnO guard bed serves as protection against a breakthrough of sulfur compounds (especially H_2S) and is operated at temperatures between 300 and 350 °C.

Table 1 Ultimate and proximate analyses of softwood pellets

Parameter	Softwood pellets
Water content (wt.-%)	7.2
Ash content (wt.-%$_{db}$)	0.2
Carbon (wt.-%$_{daf}$)	50.8
Hydrogen (wt.-%$_{daf}$)	5.9
Nitrogen (wt.-%$_{daf}$)	0.2
Sulfur (wt.-%$_{daf}$)	0.005
Chlorine (wt.-%$_{daf}$)	0.005
Oxygen[a] (wt.-%$_{daf}$)	43.1
Volatile matter (wt.-%$_{daf}$)	85.6
LHV (MJ/kg$_{db}$)	18.9
Ash deformation temp. (°C)	1330
Ash flow temp. (°C)	1440

[a]Calculated by difference to 100 wt.-%$_{daf}$

Fig. 5 Photo of the RME scrubber (left) and the activated carbon beds (right)

2.4 Fluidized bed methanation setup

Figure 6 depicts a 3D-CAD drawing of the reactor (left) and a picture of the fluidized bed methanation setup (right) at TU Wien. The reactor is designed for an SNG output of 10 kW_{th} and utilizes 1.5 kg of a self-prepared 20 wt.-% NiO/Al_2O_3 catalyst with a mean particle size of 150 μm and 1.6 kg of unimpregnated Al_2O_3. Because of the catalyst dilution, the full capacity of the reactor is not used, and the SNG output is reduced to about 5 kW for the presented experiments. The reactor is separated into two individually fluidized reaction zones operated in the bubbling fluidized bed regime. The heat released by the exothermic methanation reactions is handled with an air-cooled coil and a jacket. Water vapor can be added to the preheated syngas streams to avoid carbon depositions on the catalyst. Alternatively, hydrogen from gas cylinders can be added to the syngas prior to the methanation reactor. The gas composition can be analyzed either downstream of the hydrogen addition or in the raw-SNG downstream of the methanation reactor. A programmable logic controller records all measured temperatures, pressures, and gas analysis measurements and controls the heating tapes and cartridges. Further information on the reactor concept and the catalyst is documented in [20].

2.5 Measurement equipment

The overall process chain is equipped with more than 130 temperature and 80 pressure measurement points. Additionally, 27 gas analysis channels allow the simultaneous logging of the product gas, flue gas, and raw-SNG compositions with Rosemount NGA-2000 modules. In the product gas and the raw-SNG, the H_2, CO, CO_2, CH_4, and O_2 concentrations are measured. A PerkinElmer ARNEL – Clarus 500 gas chromatograph additionally measures ethylene, ethane, propane, and nitrogen concentrations every 12 min. Additionally, CO_2, CO, and CH_4 concentrations are redundantly measured as well. Tar sampling is performed with adapted standardized equipment, following the tar protocol (DIN CEN/TS 15,439). Single tar components are measured by gas chromatography linked with a mass spectrometer (GCMS). NH_3 is detected through wet chemical analysis with similar sampling equipment and sulfuric acid as a solvent. A more detailed description of the tar and NH_3 measurement procedure at the 100 kW_{th} pilot plant is documented in [37]. Sample bags are used for the offline measurement of H_2S with a second PerkinElmer ARNEL – Clarus 500 gas chromatograph.

2.6 Process simulation and key performance indicators

The process simulation tool IPSEpro is used to validate the measurement values by calculation of mass and energy balances and key performance indicators (KPIs). To this end, the whole process chain is modeled and set up in IPSEpro. The measured temperatures, pressures, and gas compositions in the single process units are the basis for the simulation. Furthermore, measured mass flows of the biomass input, the gasification and fluidization agent, the combustion air, the product gas and flue gas amounts, and the syngas amount in the SNG chain are used. Due to this over-specified equation system, the results in this paper represent the balanced solution from process simulation and not the raw measurement values (except where explicitly stated). Therefore, single test runs are evaluated, and no repetitions are carried out.

An important operating parameter of the DFB gasification plant is the steam-to-fuel ratio (φ_{SF}) (Eq. 1). It is defined as the amount of steam and the amount of fuel water in relation to the amount of dry and ash-free fuel introduced to the GR.

Fig. 6 3D-CAD drawing of the fluidized bed methanation reactor (left) and photo of the setup at TU Wien (right)
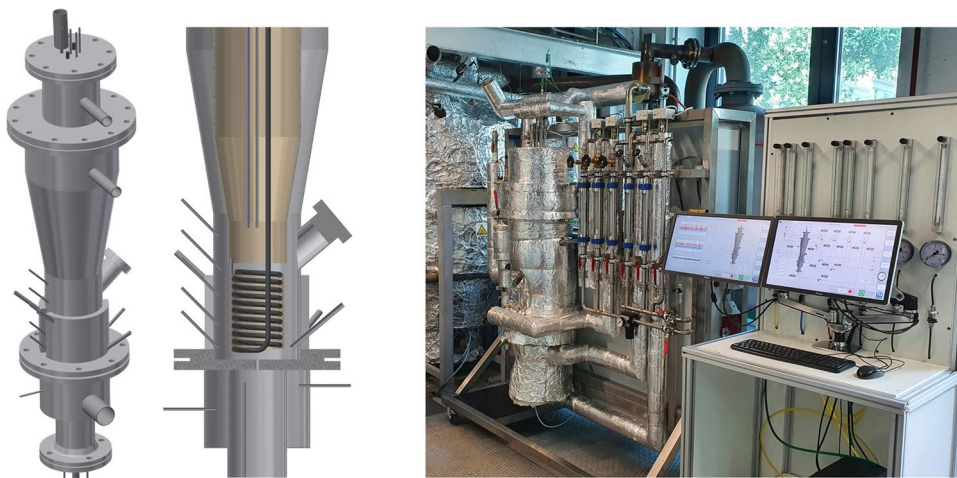
$$\varphi_{SF} = \frac{\dot{m}_{steam,GR} + \dot{m}_{H_2O,GR,fuel}}{\dot{m}_{GR,fuel,daf}} \quad (1)$$

Equation 2 shows the definition of the overall cold gas efficiency for the DFB system ($\eta_{CG,o,DFB}$). It relates the chemical energy of the product gas based on the lower heating value with the chemical energy of the fuel introduced to the GR as well as the additional fuel introduced to the CR. The relatively high heat losses of the pilot plant compared to industrial-sized gasification plants are subtracted in this equation.

$$\eta_{CG,o,DFB} = \frac{P_{PG}}{P_{GR,fuel} + P_{CR,fuel} - \dot{Q}_{loss,DFB}} * 100 \quad (2)$$

Important KPIs concerning the methanation section are displayed in Eqs. 3–7. The methane yield (Y_{CH_4}) is calculated according to Eq. 3, where $\dot{n}$ is the molar flow, and N is the number of carbon atoms in the respective gas component in the feed gas (*feed*) and the raw-SNG (*out*). Equations 4, 5, and 6 define the CO conversion (X_{CO}), the CO_2 conversion (X_{CO_2}), and the H_2 conversion (X_{H_2}), respectively.

$$Y_{CH_4} = \frac{\dot{n}_{CH_4,out}}{\sum_i N_i \dot{n}_{i,feed}} * 100 \quad (3)$$

$$X_{CO} = \frac{\dot{n}_{CO,feed} - \dot{n}_{CO,out}}{\dot{n}_{CO,feed}} * 100 \quad (4)$$

$$X_{CO_2} = \frac{\dot{n}_{CO_2,feed} - \dot{n}_{CO_2,out}}{\dot{n}_{CO_2,feed}} * 100 \quad (5)$$

$$X_{H_2} = \frac{\dot{n}_{H_2,feed} - \dot{n}_{H_2,out}}{\dot{n}_{H_2,feed}} * 100 \quad (6)$$

The stoichiometric number (SN) (Eq. 7) evaluates the product gas in terms of its stoichiometry for methanation. It relates the hydrogen content to the content of carbonaceous species to be methanated according to the corresponding reaction equations.

$$SN = \frac{y_{H_2}}{3y_{CO} + 4y_{CO_2} + 2y_{C_2H_4}} \quad (7)$$

The overall process chain is evaluated through the overall cold gas efficiency ($\eta_{CG,o}$) according to Eq. 8. It relates the chemical energy of the raw-SNG to the chemical energy of the fuel input to the GR and the CR minus heat losses (equal to Eq. 2) plus the chemical energy introduced through the external hydrogen addition.

$$\eta_{CG,o} = \frac{P_{RawSNG}}{P_{GR,fuel} + P_{CR,fuel} - \dot{Q}_{loss,DFB} + P_{H_2}} * 100 \quad (8)$$

Equation 9 shows the carbon utilization efficiency (η_C), which assesses the amount of carbon in the CH_4 of the raw-SNG compared to the amount of carbon introduced via the fuel in the GR.

$$\eta_C = \frac{\dot{m}_{C,CH_4,RawSNG}}{\dot{m}_{C,GR,fuel}} * 100 \quad (9)$$

3 Results and discussion

3.1 Operating parameters of the different process configurations

Table 2 summarizes the main operating conditions for the DFB gasification and SER process chains. Since the hydrogen addition (DFB + H_2) was carried out during the same steady-state gasification operating point as the direct methanation of the DFB product gas (DFB-Std), the operating conditions of the DFB gasification and gas cleaning parts are valid for both configurations (Sects. 3.2 and 3.3).

In general, all units are operated around atmospheric pressure. The mean temperature in the lower GR is a mean value of 7 thermocouples placed along the height of the bubbling fluidized bed. The temperature in the upper GR is the temperature where hot bed material from the CR re-enters the gasification reactor from the upper loop seal. In the CR, the given temperature is a mean value of the temperature where oil is introduced (cf. Figure 4, fuel to CR) and the temperature at the exit of the CR. Both the GR and the CR temperatures are lower in the case of the SER process to enable in situ CO_2 removal. The high additional fuel input power to the CR for DFB gasification results from the relatively high gasification temperatures and the high heat losses of the 100 kW$_{th}$ DFB pilot plant. A much lower amount for the SER process is sufficient because of the lower operating temperatures. A steam-to-fuel ratio of 0.8–0.95 is typical for this pilot plant [32]. It is based on the amount of steam required to drive the gasification reactions and the amount of steam required to fluidize the bed material. The RME scrubber was operated at a temperature of 18 °C and 36 °C with a relatively high solvent-to-gas ratio in both cases, typical for laboratory-sized columns [38]. The higher scrubber temperature for the SER process results from the higher steam content in the product gas and therefore increased water condensation enthalpy in the scrubber. The activated carbon adsorbers are operated at a slightly

Table 2 Operating parameters of the DFB gasification and SER process configurations

Parameter	DFB gasification	SER process
DFB gasifier		
Bed material mixture (wt.-%)	80/20 olivine/limestone mixture	100 limestone
Feedstock	Softwood pellets	Softwood pellets
Mean temperature lower GR (°C)	836	681
Temperature upper GR (°C)	962	778
Mean temperature CR (°C)	1015	880
Fuel input GR (kW)	91	96
Fuel input CR (kW)	52	13
φ_{SF} (kg$_{H2O}$/kg$_{fuel,daf}$)	0.80	0.95
Gas cleaning		
Particle filter temperature (°C)	258	252
Scrubber gas exit temperature (°C)	18	36
Scrubber solvent to gas ratio (kg$_{RME}$/kg$_{PG}$)	127	152
Activated carbon bed 1 temperature (°C)	51	50
Activated carbon bed 2 temperature (°C)	51	50
ZnO guard bed temperature (°C)	351	325
Methanation		
WHSV (Nl/g$_{cat}$ h)	1.3	1
Mean reaction temperature (°C)	361	342
H_2O input concentration (vol.-%)	25	5.7
Raw-SNG output (kW)	4.1	5.6
Fluidization number (U/U$_{mf}$)	5.9	3.7

elevated temperature at about 50 °C and the ZnO guard bed at about 325–350 °C to enable sufficient kinetic activity. In the fluidized bed methanation reactor, the mean temperature is set to the temperature where the CH_4 content is maximized. The mean value is computed from 5 thermocouples which are laterally and radially distributed in the catalytic bed (see [20]). For the methanation of the DFB product gas, the optimal temperature is around 360 °C, and for the SER process around 340 °C. In order to prevent carbon depositions on the catalyst, water vapor is added to the feed gas of the methanation reactor for the direct methanation of the DFB product gas. The amount is a trade-off between thermodynamic considerations and the resulting gas composition. Water is a reaction product of the Sabatier reaction and therefore influences the raw-SNG gas composition. A lower feed water content would increase the methane content in the raw-SNG and vice versa, as was shown in [20] and [39]. However, a lower feed water content might increase the carbon depositions and reduce the lifetime of the catalyst. Consequently, determining an optimal water content is a multi-objective optimization problem and thus not trivial to answer. In the case of the SER process, no additional water vapor was added to the feed gas of the methanation reactor since the hydrogen contents are considerably higher and the risk for carbon deposition is lower. Another parameter for the fluidized bed methanation reactor is the fluidization

number. The reactor is operated in the bubbling fluidized bed regime with a fluidization number between 3.7 and 6 U/U$_{mf}$, where U is the superficial gas velocity and U$_{mf}$ is the minimum fluidization velocity.

3.2 Direct methanation of the DFB product gas (DFB-Std)

This section shows the results of the full process chain for the direct methanation of the DFB product gas without external hydrogen addition. Figure 7 depicts the raw gas analysis values for the main components of the product gas of the DFB gasifier (top) and the raw-SNG (bottom) on a dry and nitrogen-free basis over time. Nitrogen is excluded because it results from flushing the fuel hoppers and the pressure measurement points, while hardly any nitrogen is expected from the fuel in the case of softwood pellets. Investigations not depicted in the current study showed that CO_2 can be used as a flushing agent, which reduces the nitrogen content in the product gas close to zero. Both the product gas and the raw-SNG compositions show a stable trend over the displayed 8.5 h. The excluded parts of the diagram are mainly caused by the maintenance of the gas measurement equipment, while the process itself remains in a steady state (see temperature trends in the supplementary material). Other excluded parts in the
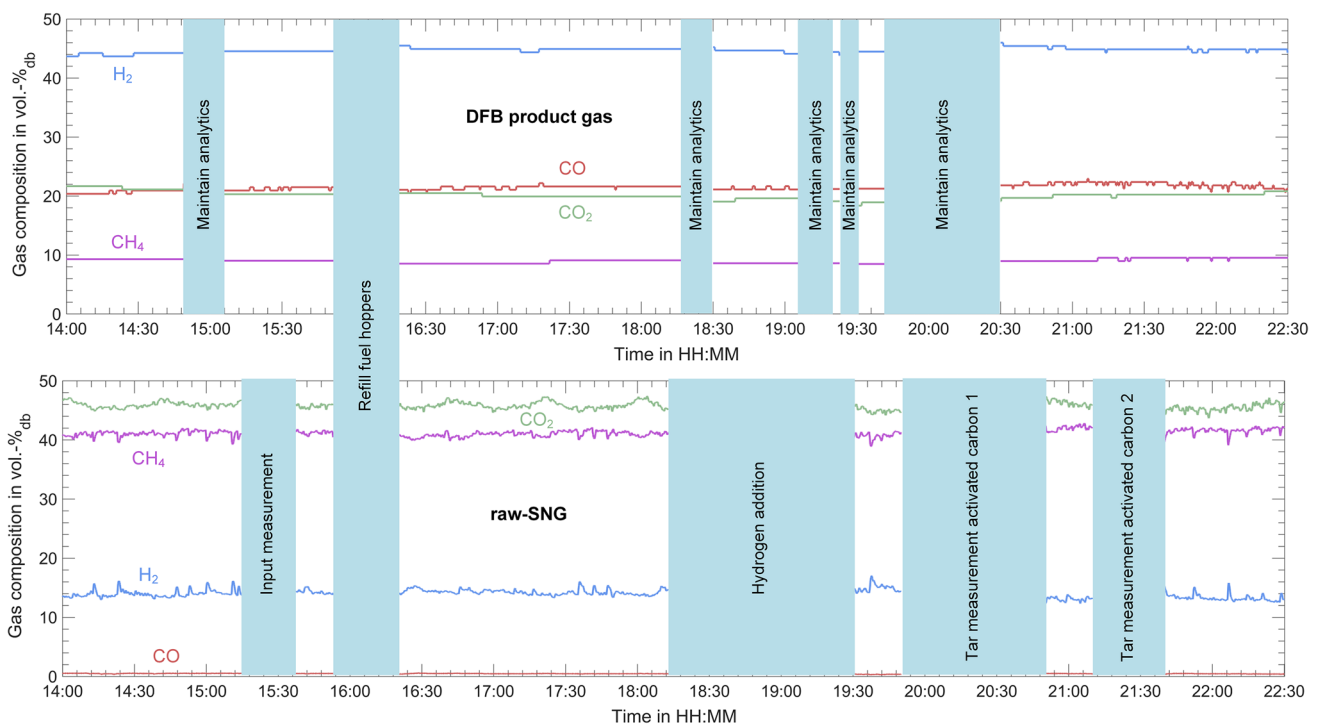
Fig. 7 Raw measurement values of the DFB product gas composition (top) and the raw-SNG composition (bottom) on a dry and nitrogen-free basis over time

raw-SNG measurement were caused by parameter variations, measuring the input gas to the methanation reactor, and tar measurements after the activated carbon filters. The latter causes a reduction in volume flow to the methanation reactor. The only interruption of the process was caused by refilling the fuel hoppers. The product gas has a comparably high hydrogen content, which is attributed to the limestone in the bed material and the relatively high gasification temperatures. Similar values were reported by Schmid et al. [32] for the 100 kW$_{th}$ DFB pilot plant. In the raw-SNG, CO_2 constitutes the main component, followed by CH_4. Residual H_2 also remains in the raw-SNG, while CO is almost completely converted. For process simulation and the mean values of the parameters in Table 2, the time frame between 16:30 and 22:30 is evaluated. Prior to that, the process is not fully in a steady state, as the CO concentration in the product gas and the temperatures in the GR show.

Figure 8a depicts the evolution of temperature and pressure (top) and gas compositions (bottom) at different positions along the process chain (stream numbers 1–12) for the validated steady-state operation between 16:30 and 22:30. Each displayed stream number can be allocated to a certain point in the process chain according to the process flow diagram in Fig. 8b). The illustration of the gas composition is divided into two sections: from stream 1–8, the evolution of impurities such as BTEX, GCMS tar, NH_3, and H_2S are

depicted, while for stream 9–12, the evolution of the main gas components (H_2, CO_2, CO, CH_4) and the water content is displayed. The illustration of impurities and main gas components for the other stream numbers is omitted because the gas composition does not change there. Furthermore, the impurity concentrations are displayed on a logarithmic scale, where the minimum value on the axis indicates that the lower detection limit is reached (bdl = below detection limit, see supplementary material for quantification of limits). Actual measurement values are indicated by marks and the corresponding measured value.

The product gas leaves the DFB system (no. 1) at 838 °C and is cooled in the radiation cooler. At this point (no. 2), gas measurements are taken. H_2S concentrations are quite low because of the high quality of the fuel and agree well with reported values [32]. GCMS tar concentrations are also low because of the high gasification temperatures and the limestone share in the bed material. The components and concentrations of the GCMS tar are listed in the supplementary material. BTEX amounts to the highest share of impurities in the product gas at roughly 4000 ppm$_{v,db}$. For all BTEX measurements, the sum is only comprised of benzene and toluene since ethylbenzene and xylene were below the detection limits. The main gas composition is also measured at this point. Since the dry main gas composition does not change, the values at stream no. 10 can be taken, where the main gas composition is redundantly measured.
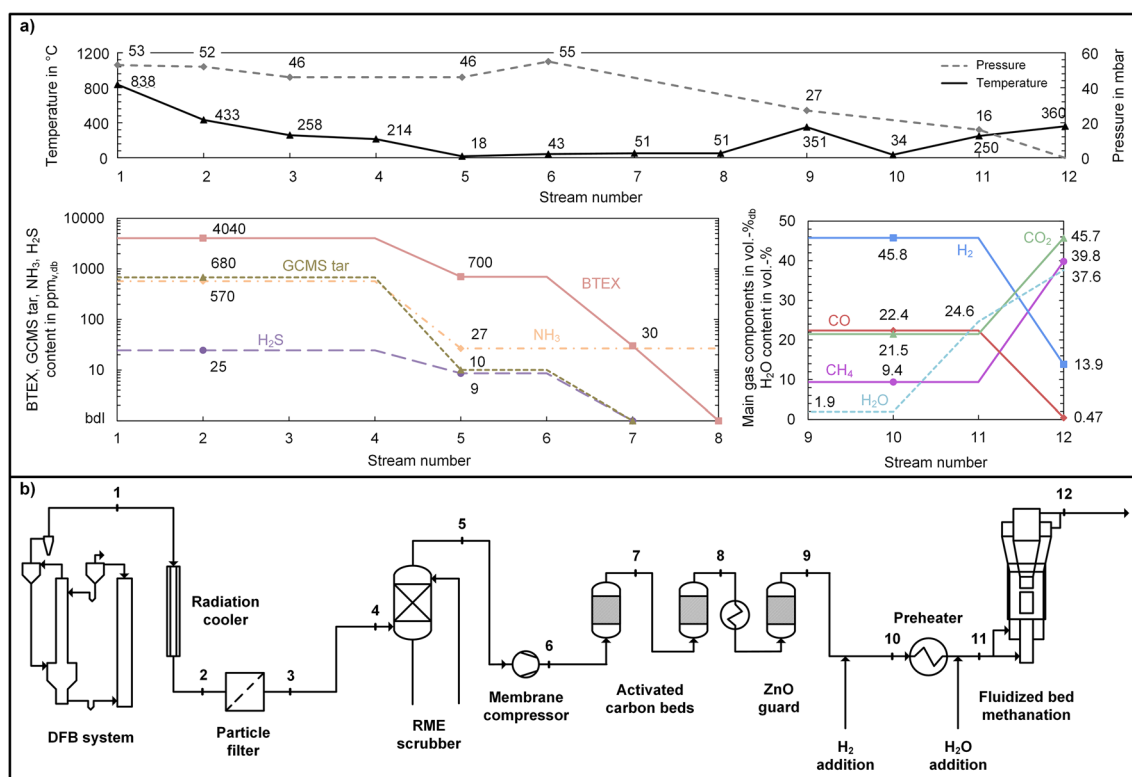
Fig. 8 Process conditions over the whole process chain during the direct methanation of the DFB product gas: **a** evolution of temperature, pressure (top), and concentration of impurities and main gas components (bottom), **b** process flow diagram with stream numbers, see supplementary material for detection limits

In the particle filter, dust and char particles are removed at around 260 °C before the gas enters the RME scrubber at a slightly lower temperature due to heat losses (no. 4). Entering the scrubber at this temperature level ensures that no tar components condensate in the particle filter or the piping. The gas leaves the scrubber at 18 °C with a reduced amount of impurities (no. 5). Especially GCMS tar concentrations are reduced by a large margin through condensation and dissolution in the RME (98.5% separation efficiency). Naphthalene, which makes up two-thirds of the GCMS tar concentration, is removed below the detection limit. NH_3 is a water-soluble molecule and is also efficiently removed (95% separation efficiency) in the scrubber through dissolution in the condensed water vapor. Assuming water saturation at the exit of the scrubber leads to a calculated water content of 1.9 vol.-% (see stream no. 9). BTEX components are reduced by 83%. Because benzene has a lower boiling point than toluene, the remaining BTEX sum mainly consists of benzene, while toluene is almost completely removed. The high separation efficiencies in the scrubber are attributed to the relatively low operating temperatures (18 °C) and the high solvent-to-gas ratio. Literature reports a substantial variation of separation efficiencies in the RME scrubber based on the applied operating conditions. Laboratory-sized columns

operated at a high solvent-to-gas ratio and at temperatures below 10 °C report almost complete NH_3 [40] and tar [38] separation efficiencies. At an industrial scale, operating temperatures are usually higher due to technical limitations and economic considerations, which considerably limit the separation efficiencies [37, 38]. Furthermore, the H_2S concentration is reduced in the scrubber as well.

The membrane compressor is used to set the required volume flow and to overcome pressure losses throughout the process chain—no pressurized operation is intended. Since the DFB system is operated at a slight overpressure of around 50 mbar, the membrane compressor only increases the pressure marginally (no. 6). The activated carbon beds further reduce the concentrations of the impurities and are operated at around 50 °C. GCMS tar and H_2S concentrations are reduced below the detection limit in the first bed (no. 7). However, 30 $ppm_{v,db}$ of toluene is still measured after the first bed and removed below the detection limit in the second bed (no. 8). NH_3 has not been measured after the activated carbon beds and is assumed to pass through unaffected. Since no H_2S breakthrough was detected, the ZnO guard bed only acts as an additional security layer. A temperature reduction after the ZnO guard bed (no. 10) and a consecutive preheating (no. 11) is required because of the volume flow measurement

with a gas meter in this particular case. In an industrial plant, the sensible heat after the ZnO guard bed could be directly utilized as preheating for the methanation reactor. After the preheater, steam is added to the syngas at 250 °C (no. 11) to shift the gas in the methanation reactor towards H_2. In the methanation reactor, syngas is converted to raw-SNG (no. 12). A methane content of about 40 vol.-%$_{db}$ is achieved. The high CO_2 content is a result of the water–gas shift reaction and the substoichiometric product gas composition (concerning SN), which leads to the production of CO_2 in the methanation reactor. For the same reason, and because of thermodynamic and kinetic limitations, residual H_2 remains in the raw-SNG, while CO is almost completely converted.

Seemann et al. [41] achieved similar results applying fluidized bed methanation of a partial product gas flow from the DFB gasifier in Güssing, Austria. They operated the fluidized bed reactor at 385 °C and 3 bar$_a$ at 4.5 Nl/g_{cat} h with a commercial 50 wt.-% Ni/γ-Al_2O_3 catalyst. However, the product gas composition from the DFB gasifier in Güssing differs from the advanced DFB pilot plant. The DFB Güssing product gas shows a lower H_2 and CO_2 content and a higher CO content, which leads to an overall lower stoichiometric number. Because of the deviating product gas composition and different operating conditions, their raw-SNG shows a slightly higher CH_4 content and an increased CO_2 content, while the H_2 content is lower. Especially a pressurized operation, which could be performed in this case, in combination with the lower stoichiometric number, allows a suppression of the H_2 content in the raw-SNG. On the other hand, a pressurized application requires compression energy and pressure vessels according to the pressurized equipment directive.

3.3 Methanation of the DFB product gas with external hydrogen addition (DFB + H_2)

This section shows the results of the product gas methanation with external hydrogen addition. Hydrogen addition was performed during the same steady-state gasification experiment already presented in Sect. 3.1. Therefore, only the results of the methanation part are discussed. Table 3

Table 3 Operating parameters of the methanation reactor

Parameter	SN = 0.91	SN = 1.04
WHSV (Nl/g_{cat} h)	1.8	2.0
Mean reaction temperature (°C)	358	364
Raw-SNG output (kW)	7.6	8.4
Fluidization number (U/U_{mf})	6.2	6.9
H_2 addition (vol.-%)[a]	91	111
Water addition (vol.-%)	0	0

[a]In vol.-% of the amount of syngas upstream H_2 addition

lists the main operating parameters for two different operating points. The operating points differ in terms of the amount of hydrogen added to the product gas before methanation, which is represented by the stoichiometric number (SN = 0.91 and SN = 1.04). Through the additional hydrogen amount, the WHSV and the fluidization number in the methanation reactor increase compared to the direct methanation of the product gas and the raw-SNG output approximately doubles. The reaction temperature and pressure are kept constant at approximately 360 °C and 1 bar$_a$, respectively. Because of the high hydrogen content and the roughly stoichiometric composition, no additional steam is added to the feed gas of the methanation reactor.

Figure 9 depicts the evolution of the gas composition over stream nos. 9–12 for the two different operating points. Figure 9a shows the operating point with less hydrogen (SN = 0.91). Between stream nos. 9 and 10, hydrogen is added to the product gas, which increases the hydrogen content to 72 vol.-%$_{db}$ and dilutes the other gas components. The raw-SNG after the methanation reactor (stream no. 12) consists mainly of methane as well as a significant amount
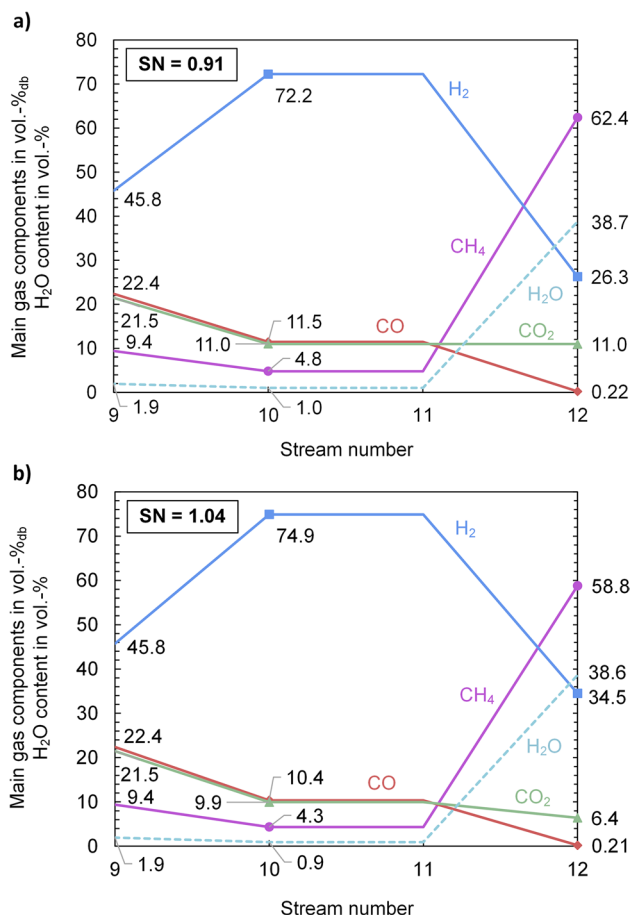
Fig. 9 Evolution of main gas components over the methanation reactor (stream nos. 9–12) for DFB + H_2: **a** SN = 0.91, **b** SN = 1.04

of residual hydrogen and carbon dioxide. Coincidentally, the volume percentage of CO_2 remains the same before and after methanation because of the volume contraction during the reaction. A CO_2 conversion nevertheless takes place, as Fig. 10 elucidates. Carbon monoxide, on the other hand, is converted to a large extent.

Figure 9b shows the operating point with a higher amount of hydrogen added (SN = 1.04). In comparison, this leads to lower methane and higher residual hydrogen contents compared to SN = 0.91. Carbon dioxide is further reduced, while the residual CO content remains almost unaffected.

3.4 Direct methanation of the SER product gas

The SER process allows an adaption of the product gas composition towards higher hydrogen contents via in situ CO_2 removal, as explained in Fig. 2 (right). No additional hydrogen was added to the product gas. Figure 10 depicts the raw gas analysis values for the main components of the SER product gas (top) and the raw-SNG (bottom) on a dry and nitrogen-free basis. The gas compositions show constant mean values over the displayed 105 min but increased instabilities on a lower time scale compared to DFB gasification. An H_2 content of about 60 vol.-%$_{db}$ could be reached in the product gas, whereas the CO and CO_2 concentrations are lowered to around 11 vol.-%$_{db}$ compared to DFB-Std. CH_4 is somewhat increased to around 13 vol.-%$_{db}$ because of the

reduced product gas volume flow due to the CO_2 removal. Hence, the product gas composition is much closer to the requirements of the methanation reactions without the need for additional hydrogen compared to the product gas of DFB gasification. Therefore, also the CH_4 content in the raw-SNG is elevated to around 70 vol.-%$_{db}$, the rest being residual contents of H_2 and CO_2. Only trace amounts of CO remain in the raw-SNG.

To track the temperatures, pressures, gas compositions, and impurity concentrations, Fig. 11 depicts the via mass and energy balancing validated data at different positions along the SER process chain in analogy to Fig. 8. Because of the SER operation mode of the gasifier, the temperatures at the exit of the gasifier, and therefore after the radiation cooler, are lower (stream nos. 1 and 2). GCMS tar and BTEX concentrations differ from the DFB gasification process chain because of the catalytically active bed material on the one hand and the lower gasification temperatures on the other hand. The GCMS tar components and concentrations are again listed in the supplementary material. Despite using the same softwood pellets in the DFB gasification and the SER process chains, the NH_3 concentration is higher for the latter. This is because of the lower gasification temperatures plus the in situ CO_2 removal and thus a lower volume flow of dry product gas from the gasifier in the case of the SER process. In the filter and entry to the RME scrubber, temperatures are similar to the DFB gasification. However, the
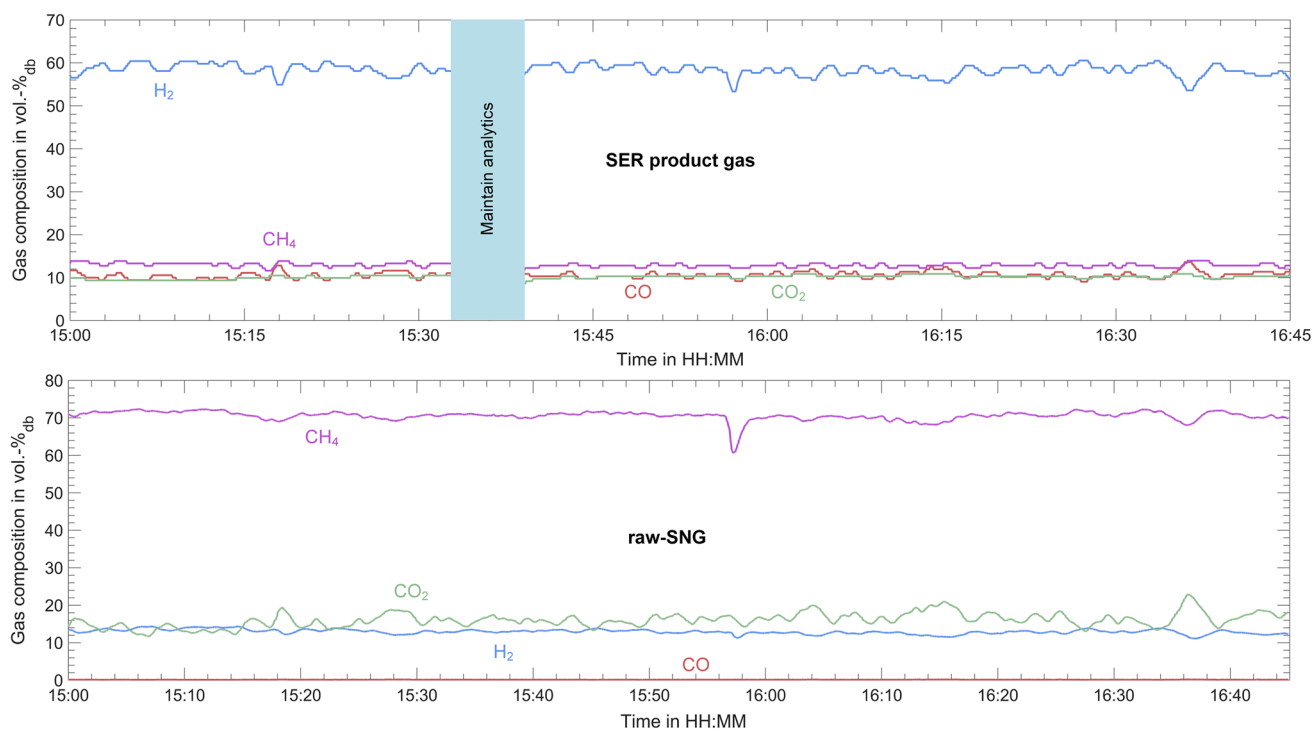

Fig. 10 Raw measurement values of the SER product gas composition (top) and the raw-SNG composition (bottom) on a dry and nitrogen-free basis over time
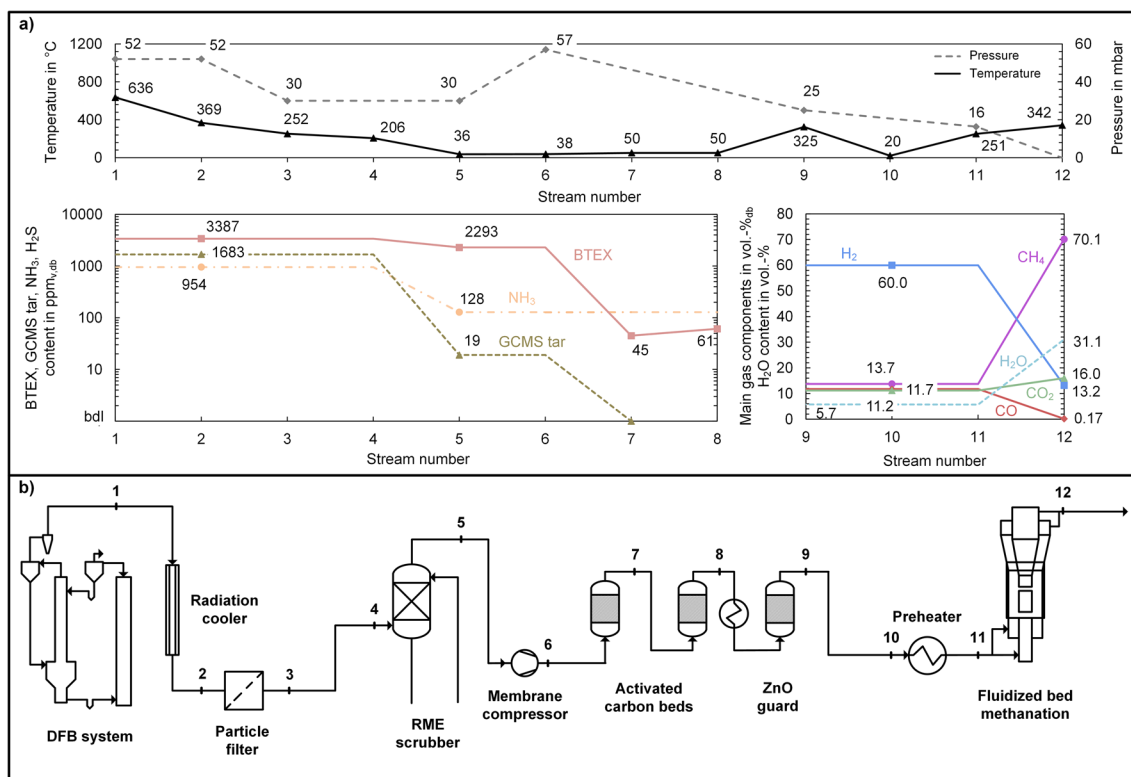
Fig. 11 Process conditions over the whole process chain during the direct methanation of the SER product gas: **a** evolution of temperature, pressure (top), and concentration of impurities and main gas components (bottom), **b** process flow diagram with stream numbers, see supplementary material for detection limits

exit temperature of the RME scrubber (no. 5) is elevated to 36 °C due to the increased steam content in the product gas for the SER process and thus a higher condensation enthalpy. At a constant cooling power of the scrubber, this leads to an elevated exit temperature and thus a higher residual water content in the scrubbed product gas. GCMS tars, BTEX and NH_3 are again reduced in the scrubber. However, the increased operating temperature of the scrubber leads to a reduced separation efficiency of BTEX and NH_3 at 32% and 87%, respectively. The separation efficiency of GCMS tar is unaffected by the increased operating temperature. In the activated carbon adsorbers, residual GCMS tar components are removed and BTEX concentrations are further reduced. However, no full removal of BTEX was possible in this case. Toluene was detected after the first and the second activated carbon bed (nos. 7 and 8). The DFB gasification process chain already showed a breakthrough of toluene through the first activated carbon bed. For the SER process chain, the increased water vapor content in the scrubbed product gas might have further lowered the adsorption capacities of the activated carbon. The increase of the toluene concentration from the first to the second bed might even indicate the desorption of toluene. In the methanation reactor, the syngas (no. 10) is converted to raw-SNG (no. 12) after preheating

(no. 11). A high methane content of 70 vol.-%$_{db}$ is reached while the H_2 concentration drops to 16 vol.-%$_{db}$ and only 0.17 vol.-%$_{db}$ of CO remains. Part of the CO_2 is also converted, but the concentration actually increases because of the volume reduction of the methanation reactions.

3.5 Comparison of the process chains

For a comparison of the different process chain configurations, the raw-SNG gas composition (Fig. 12a)) and the KPIs of the methanation reactor (Fig. 12b)) are displayed. A substantial increase in methane content and a decrease in carbon dioxide content result from the externally added hydrogen ($DFB + H_2$) and the methanation of the SER product gas (SER). Concurrently, the methane yield and the CO_2 conversion increase. While the highest methane content is reached for the substoichiometric SER product gas (SN = 0.71), the methane yield is higher for $DFB + H_2$ because of the higher SN. The lower methane content for SN = 0.91 and SN = 1.04 results from the dilution with a higher amount of residual hydrogen. In the case of the DFB-Std process chain (SN = 0.30), CO_2 is produced from CO and H_2O through the water–gas shift reaction in the methanation reactor. With hydrogen addition and the SER product gas, CO_2 is actually
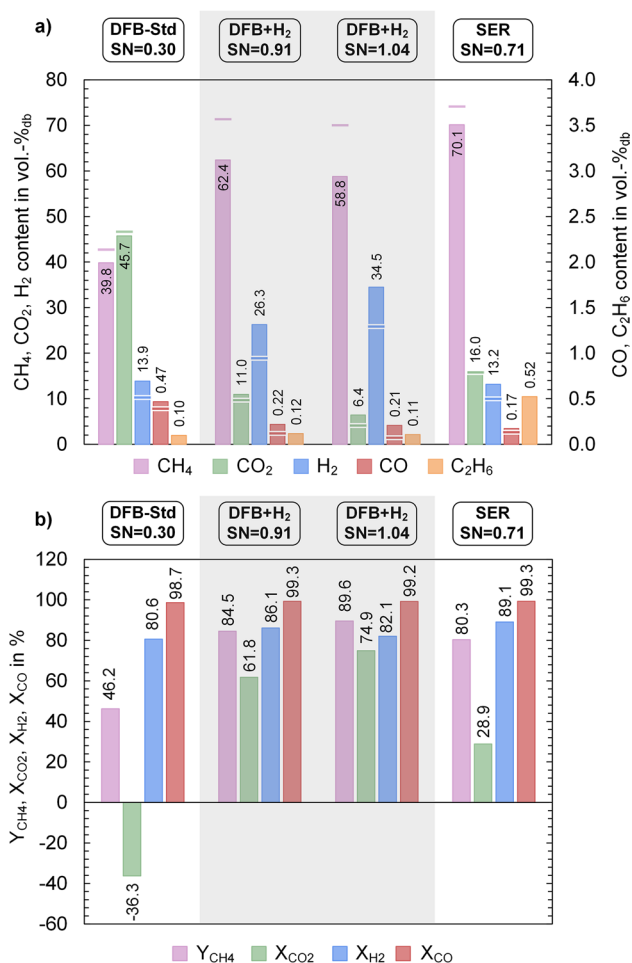
Fig. 12 Comparison of the three operating points: **a** raw-SNG composition, **b** KPIs of the methanation reactor

converted. The higher the amount of hydrogen at the inlet of the methanation reactor, the higher the CO_2 conversion. Residual hydrogen contents in the raw-SNG increase with an increasing amount of hydrogen in the syngas. Hydrogen conversion is, however, higher for the SER configuration, followed by SN = 0.91 and SN = 1.04. DFB-Std operation yields the lowest hydrogen conversion because the added steam to the product gas shifts the raw-SNG towards H_2 and CO_2 according to the water–gas shift reaction. CO is almost completely converted for all operating points. Nevertheless, the DFB + H_2 and SER process chains allow a further reduction of the CO content and a slight increase in CO conversion. Some ethane is detected in the raw-SNG, which results from the conversion of ethylene to ethane and possibly the ethane in the product gas itself. The ethane content in the raw-SNG is similar for all three DFB gasification operating points but higher for the SER configuration because of the higher ethylene content in the SER product gas.

Figure 12a additionally depicts the theoretical composition of the raw-SNG in the thermodynamic equilibrium,

denoted by horizontal bars. In the case of DFB-Std and SER product gas methanation, the measured composition is close to the thermodynamic limit. For the two DFB + H_2 operating points, a larger deviation from the maximum values can be seen. Especially methane and hydrogen contents deviate from thermodynamic predictions, and a further conversion would have been theoretically possible. In this case, the higher WHSV and, therefore, a lower residence time resulting from hydrogen addition most likely lead to a kinetic limitation of the reaction. In general, the results agree very well with investigations carried out with synthetically pre-mixed syngases in the same methanation reactor [20]. In general, the raw-SNG compositions of the DFB + H_2 and SER process configurations are much closer to the requirements of the natural gas grid. However, a further conversion of H_2, CO_2, and CO would still be necessary. This could be achieved at lower reaction temperatures or a pressurized operation. Theoretical calculations show that adapted operating conditions can lead to a grid-feedable SNG for the SER [18, 19] and the DFB + H_2 [22] configurations. Excessive separated hydrogen, e.g., via membrane separation, could be recirculated to the inlet of the methanation reactor. Alternatively, a second-stage methanation reactor with intermediate water condensation could also enhance conversion rates to reach grid specifications. This possibility was already shown for biogas upgrading to SNG with additional hydrogen [42].

For the performance of the methanation reactor alone, it is unimportant how the adjustment of the syngas towards high H_2 contents is achieved. The main influencing parameter is the SN at the inlet of the methanation reactor and, to some extent, the changing WHSV due to H_2 addition. However, the performance of the whole process chain depends very much on the origin of the syngas. Therefore, to compare the KPIs of the whole process chain, Fig. 13 depicts the overall cold gas efficiency ($\eta_{CG,o}$) and the carbon utilization efficiency (η_C). Interestingly, $\eta_{CG,o}$ is very similar for the DFB-Std and the DFB + H_2 operating points at 58 to 59%. Large-scale industrial plants, like GoBiGas and Güssing, report similar values at a maximum of 62–63% [8, 43]. However, a fair comparison is hardly possible. On the one hand, large-scale gasifiers perform at a higher cold gas efficiency than the pilot-scale plant at TU Wien. On the other hand, upgrading the raw-SNG to grid-feedable SNG is experimentally not investigated in this paper. This would reduce the cold gas efficiency, even if the excessive hydrogen is recirculated to the feed of the methanation reactor. For the SER process configuration, on the other hand, a higher cold gas efficiency results from this setup. Compared to DFB gasification, the gasification and combustion temperatures for SER are lower, and more char is available for combustion. Therefore, the amount of additional fuel needed in the combustion reactor is much lower, increasing the overall cold gas efficiency. Brellochs [19] calculates an overall cold gas efficiency of
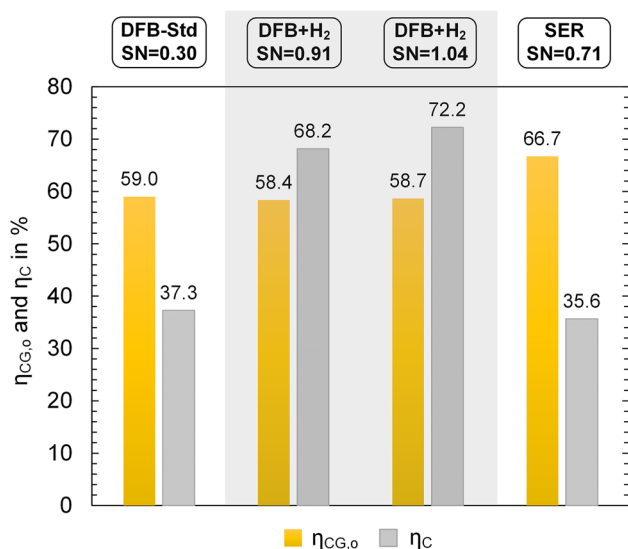
Fig. 13 Comparison of the KPIs of the overall process chain for the three operating points

67.5% for a 10 MW$_{th}$ SNG plant based on a process simulation of the SER process, which is close to the calculated 66.7% in this study. For the DFB + H$_2$ process, simulations carried out by Gassner and Maréchal [9] and Alamia et al. [22] result in values between 67 and 73%. These values are considerably higher than in this study, which is a result of the limited conversion in the methanation reactor. Furthermore, the same limited comparability between small and large-scale installations remains, as discussed above.

The carbon utilization efficiency at 37% for the DFB-Std product gas methanation is within the expected range following theoretical considerations [18]. Larsson et al. [8] state a somewhat lower η_C at around 30% for the large-scale GoBiGas plant. This can be explained by the product gas recirculation to the combustion reactor to compensate for the heat demand in the gasifier in large-scale plants, which is not carried out at pilot scale. The SER process configuration shows a similar, slightly lower η_C. Most of the carbon is lost through char combustion and the calcination of CaCO$_3$ in the CR of the DFB system. The carbon in the CaCO$_3$ needs to be sacrificed to achieve a H$_2$-enriched product gas through the CO$_2$ removal in the GR. Some carbon is also lost through the remaining CO$_2$ in the raw-SNG and the separated tar in the scrubber.

Through the addition of hydrogen, a significant increase of η_C to roughly 70% is possible. More hydrogen addition (SN = 1.04) leads to a higher carbon utilization than less hydrogen addition (SN = 0.91), which was already indicated by the methane yield in Fig. 12. The remaining carbon is again lost through char combustion in the CR and to some extent through the remaining CO$_2$ in the raw-SNG and the separated tar in the scrubber.

In this study, the investigations were carried out with softwood pellets as a comparable reference fuel for all process configurations. However, the type and quality of biomass can have a major impact on the product gas quality and thus on the required gas cleaning and the raw-SNG composition. For example, Schmid et al. [32] and Schweitzer et al. [44] show that different fuels like bark, hazelnut shells, sugar cane bagasse, or sewage sludge have an impact on the product gas composition and on the concentration of impurities in particular. Residual materials typically exhibit higher concentrations of nitrogen and sulfur-containing compounds which necessitates a more rigorous gas cleaning section. The impact of different fuels on the raw-SNG composition is, for example, discussed by Bartik et al. [18]. Besides the feedstock, water is another important resource for the process. Steam is required as a gasification and fluidization agent in the GR and for the production of H$_2$ through electrolysis. Nevertheless, the overall water consumption of the process can be kept to a minimum through process integration. For large-scale applications, the separated water phase from the RME scrubber can be reused as a gasification agent. Similarly, the water fraction resulting from condensation and gas drying during the upgrading of raw-SNG can be reused within the process. However, a more detailed insight into different feedstocks and the water balance would go beyond the scope of this paper.

Overall, the comparison reveals the strengths and weaknesses of the different process configurations. As a decision basis, Table 4 lists a summary of the main advantages and disadvantages of the three process configurations.

4 Conclusions

In this work, advanced process chains for raw-SNG production were experimentally investigated and compared on a pilot scale and measured analytical values were validated with the aid of process simulation. A 100 kW$_{th}$ advanced DFB gasification reactor was coupled with gas cleaning units and a 10 kW$_{th}$ fluidized bed methanation reactor. External hydrogen addition allowed the investigation of hybrid SNG production process chains with increased carbon utilization. DFB gasification with in situ CO$_2$ removal (SER process) in combination with methanation was investigated as another novel process configuration. It allowed an adaption of the product gas composition to the needs of the methanation process without the use of external hydrogen. Additionally, extensive analytical measurements allowed the tracking and quantification of impurities over the whole process chain.

The following conclusions can be drawn:

Table 4 Advantages and disadvantages of the investigated process configurations

Process configuration	Advantages	Disadvantages
DFB-Std	- Stable steady-state operation - Similar large-scale operation demonstrated [43]	- High CO_2 contents in raw-SNG (upgrading effort) - Unsuitable product gas composition for methanation - Risk of catalyst aging through carbon deposition - Steam addition to inlet of methanation reactor
DFB + H_2	- Flexible adjustment of syngas composition through H_2 addition - Doubling of carbon utilization and thus doubling of SNG amount - Less risk of catalyst aging through carbon deposition due to SN adjustment - No steam addition at inlet of methanation reactor necessary - Possibly less effort for gas upgrading required	- Costs for hydrogen production - Increase in overall system complexity due to additional process units - Renewable electricity required for ecological viable concept - Potentially fluctuating H_2 supply increases requirements on dynamic process behavior
SER	- In situ adjustment of product gas composition through SER process without the need for external hydrogen addition - Higher overall cold gas efficiency for this setup - Less risk of methanation catalyst aging through carbon deposition due to SN adjustment - No steam addition at inlet of methanation reactor necessary - Possibly less effort for gas upgrading required - Less volume flow due to in-situ CO_2 removal and thus smaller units and less electrical power consumption	- SER process not yet demonstrated on a large-scale - No increase in carbon utilization possible

(i) A stable steady-state operation of the advanced DFB gasifier in combination with the SNG process chain was demonstrated (DFB-Std). A product gas with 46 vol.-% H_2 is converted to a raw-SNG with around 40 vol.-% CH_4 with an overall cold gas efficiency of 59% without external hydrogen addition.

(ii) The incorporation of external hydrogen (DFB + H_2) allowed a more efficient utilization of the biomass carbon. With a carbon utilization efficiency of about 70%, almost twice the amount of carbon is utilized for methane production compared to the DFB-Std process chain, while the cold gas efficiency remains practically the same. Simultaneously, the H_2, CO, and CO_2 conversions are improved despite the higher WHSV compared to the DFB-Std process chain.

(iii) The SER process can be applied advantageously to catalytic methanation as an alternative to hydrogen addition or the DFB-Std process chain. It allows the adjustment of the product gas composition towards high hydrogen contents suitable for methanation without the technical limits and additional expenses of external hydrogen addition. Additionally, SNG production is feasible at a higher overall cold gas efficiency, while the carbon utilization is similar to the DFB-Std process chain.

(iv) Low concentrations of impurities in the product gas through the advanced gasification system and the high quality of the fuel were achieved. Impurity tracing through the process chain showed that the RME scrubber serves as an efficient impurity removal unit. High tar, NH_3, and BTEX separation efficiencies were achieved, but there is a dependency on the scrubber operating temperature.

(v) For grid injection, upgrading steps are necessary independent of the applied process configuration. However, the type of upgrading steps and the optimal process conditions in the methanation reactor might differ. For the DFB + H_2 and the SER process configuration, less upgrading effort might be possible given the right process conditions.

Depending on the given circumstances and the defined goals, the most suitable process configuration might differ, as Table 4 shows. DFB + H_2 might be favored if renewable hydrogen is readily available from a technical and economic perspective, and the goal is the maximization of biomass utilization. If no hydrogen is available, the SER process configuration is an interesting alternative to the DFB-Std process configuration.

Optimized process concepts, including upgrading steps and economic and ecologic comparisons of the different routes, should be investigated to provide a more precise basis for decision-making. Furthermore, SNG production from biogenic residual material would be an ecologically and economically interesting alternative.

Declarations

Ethical approval Not applicable.

Competing interests Author Hermann Hofbauer is the editor of the Journal Biomass Conversion and Biorefinery. Apart from that, the authors declare that they have no relevant financial or non-financial interests to disclose.

References

1. IEA (2021) World energy outlook 2021, IEA, Paris. https://www.iea.org/reports/world-energy-outlook-2021. Accessed 23 May 2023
2. Rönsch S, Schneider J, Matthischke S, Schlüter M, Götz M, Lefebvre J, Prabhakaran P, Bajohr S (2016) Review on methanation – From fundamentals to current projects. Fuel 166:276–296. https://doi.org/10.1016/j.fuel.2015.10.111
3. Götz M, Lefebvre J, Mörs F, McDaniel Koch A, Graf F, Bajohr S, Reimert R, Kolb T (2016) Renewable power-to-gas: a technological and economic review. Renew Energy 85:1371–1390. https://doi.org/10.1016/j.renene.2015.07.066
4. Thunman H, Seemann M, Berdugo Vilches T, Maric J, Pallares D, Ström H, Berndes G, Knutsson P, Larsson A, Breitholtz C, Santos O (2018) Advanced biofuel production via gasification – lessons learned from 200 man-years of research activity with Chalmers' research gasifier and the GoBiGas demonstration plant. Energy Sci Eng 6(1):6–34. https://doi.org/10.1002/ese3.188
5. Schildhauer TJ, Biollaz SM (2016) Synthetic natural gas from coal, dry biomass, and power-to-gas applications. Wiley, Hoboken
6. Gassner M, Baciocchi R, Maréchal F, Mazzotti M (2009) Integrated design of a gas separation system for the upgrade of crude SNG with membranes. Chem Eng Process 48(9):1391–1404. https://doi.org/10.1016/j.cep.2009.07.002
7. Mevissen N, Schulzke T, Unger CA, an Bhaird SM (2009) Thermodynamics of autothermal wood gasification. Environ Prog Sustain Energy 28(3):347–354. https://doi.org/10.1002/ep.10393
8. Larsson A, Gunnarsson I, Tengberg F (2018) The GoBiGas project - demonstration of the production of biomethane from biomass via gasification. Technical Report, December 2018. https://doi.org/10.13140/RG.2.2.27352.55043
9. Gassner M, Maréchal F (2008) Thermo-economic optimisation of the integration of electrolysis in synthetic natural gas production from wood. Energy 33(2):189–198. https://doi.org/10.1016/j.energy.2007.09.010
10. Barbuzza E, Buceti G, Pozio A, Santarelli M, Tosti S (2019) Gasification of wood biomass with renewable hydrogen for the production of synthetic natural gas. Fuel 242:520–531. https://doi.org/10.1016/j.fuel.2019.01.079
11. Grigoriev SA, Fateev VN, Bessarabov DG, Millet P (2020) Current status, research trends, and challenges in water electrolysis science and technology. Int J Hydrog Energy 45(49):26036–26058. https://doi.org/10.1016/j.ijhydene.2020.03.109
12. Dincer I (2012) Green methods for hydrogen production. Int J Hydrog Energy 37(2):1954–1971. https://doi.org/10.1016/j.ijhydene.2011.03.173
13. Karatza D, Konstantopoulos C, Chianese S, Diplas S, Svec P, Hristoforou E, Musmarra D (2021) Hydrogen production through water splitting at low temperature over Fe_3O_4 pellet: Effects of electric power, magnetic field, and temperature. Fuel Process Technol 211:106606. https://doi.org/10.1016/j.fuproc.2020.106606
14. Safari F, Dincer I (2020) A review and comparative evaluation of thermochemical water splitting cycles for hydrogen production. Energy Conv Manag 205:112182. https://doi.org/10.1016/j.enconman.2019.112182
15. Castro J, Leaver J, Pang S (2022) Simulation and techno-economic assessment of hydrogen production from biomass gasification-based processes: a review. Energies 15(22):8455. https://doi.org/10.3390/en15228455
16. Singh T, Alhazmi A, Mohammad A, Srivastava N, Haque S, Sharma S, Singh R, Yoon T, Gupta VK (2021) Integrated biohydrogen production via lignocellulosic waste: opportunity, challenges & future prospects. Bioresour Technol 338:125551. https://doi.org/10.1016/j.biortech.2021.125511
17. Fuchs J, Schmid JC, Müller S, Hofbauer H (2019) Dual fluidized bed gasification of biomass with selective carbon dioxide removal and limestone as bed material: a review. Renew Sust Energ Rev 107:212–231. https://doi.org/10.1016/j.rser.2019.03.013
18. Bartik A, Benedikt F, Lunzer A, Walcher C, Müller S, Hofbauer H (2020) Thermodynamic investigation of SNG production based on dual fluidized bed gasification of biogenic residues. Biomass Convers Biorefinery 11:95–110. https://doi.org/10.1007/s13399-020-00910-y
19. Brellochs J (2014) "Experimentelle Untersuchung und Prozess-Simulation der AER-Biomassevergasung zur Erzeugung eines regenerativen Erdgassubstitutes", Dissertation, Universität Stuttgart, 1st edn. Cuvillier, Göttingen (ISBN: 9783954048830)
20. Bartik A, Fuchs J, Pacholik G, Föttinger K, Hofbauer H, Müller S, Benedikt F (2022) "Experimental investigation on the methanation of hydrogen-rich syngas in a bubbling fluidized bed reactor utilizing an optimized catalyst. Fuel Process Technol 237:107402. https://doi.org/10.1016/j.fuproc.2022.107402
21. Gómez L, Grasa G, Martínez I, Murillo R (2022) Performance study of a methanation process for a syngas obtained from a sorption enhanced gasification process. Chem Eng Sci 267:118291. https://doi.org/10.1016/j.ces.2022.118291
22. Alamia A, Òsk Gardarsdòttir S, Larsson A, Normann F, Thunman H (2017) Efficiency comparison of large-scale standalone,

centralized, and distributed thermochemical biorefineries. Energy Technol 5(8):1435–1448. https://doi.org/10.1002/ente.201600719

23. Salbrechter K, Schubert T (2021) Combination of b-fuels and e-fuels—a technological feasibility study. Energies 14(17):5250. https://doi.org/10.3390/en14175250

24. Menin L, Vakalis S, Benedetti V, Patuzzi F, Baratieri M (2020) Techno-economic assessment of an integrated biomass gasification, electrolysis, and syngas biomethanation process. Biomass Convers Biorefinery 11(2):445–459. https://doi.org/10.1007/s13399-020-00654-9

25. Giglio E, Vitale G, Lanzini A, Santarelli M (2021) Integration between biomass gasification and high-temperature electrolysis for synthetic methane production. Biomass Bioenerg 148:106017. https://doi.org/10.1016/j.biombioe.2021.106017

26. Leimert JM, Neubert M, Treiber P, Dillig M, Karl J (2018) Combining the heatpipe reformer technology with hydrogen-intensified methanation for production of synthetic natural gas. Appl Energy 217:37–46. https://doi.org/10.1016/j.apenergy.2018.02.127

27. Witte J, Calbry-Muzyka A, Wieseler T, Hottinger P, Biollaz SM, Schildhauer TJ (2019) Demonstrating direct methanation of real biogas in a fluidised bed reactor. Appl Energy 240(2018):359–371. https://doi.org/10.1016/j.apenergy.2019.01.230

28. Pozzo M, Lanzini A, Santarelli M (2015) Enhanced biomass-to-liquid (BTL) conversion process through high temperature co-electrolysis in a solid oxide electrolysis cell (SOEC). Fuel 145:39–49. https://doi.org/10.1016/j.fuel.2014.12.066

29. Clausen LR, Houbak N, Elmegaard B (2010) Technoeconomic analysis of a methanol plant based on gasification of biomass and electrolysis of water. Energy 35(5):2338–2347. https://doi.org/10.1016/j.energy.2010.02.034

30. Hauser A, Wolf-Zoellner P, Haag S, Dettori S, Tang X, Mighani M, Matino I, Mocci C, Colla V, Kolb S, Bampaou M, Panopoulos K, Kieberger N, Rechberger K, Karl J (2022) Valorizing steelworks gases by coupling novel methane and methanol synthesis reactors with an economic hybrid model predictive controller. Metals 12(6):1023. https://doi.org/10.3390/met12061023

31. Kleiber S, Loder A, Siebenhofer M, Böhm A, Lux S (2022) Direct reduction of siderite ore combined with catalytic CO/CO₂ hydrogenation to methane and methanol: a technology concept. Chem Ing Tech 94(5):701–711. https://doi.org/10.1002/cite.202100189

32. Schmid JC, Benedikt F, Fuchs J, Mauerhofer AM, Müller S, Hofbauer H (2019) Syngas for biorefineries from thermochemical gasification of lignocellulosic fuels and residues - 5 years' experience with an advanced dual fluidized bed gasifier design. Biomass Convers Biorefinery 11:2405–2442. https://doi.org/10.1007/s13399-019-00486-2

33. Schmid JC (2014) Development of a novel dual fluidized bed gasification system for increased fuel flexibility. Dissertation, TU Wien, Vienna. https://doi.org/10.34726/hss.2014.25397

34. Karl J, Pröll T (2018) Steam gasification of biomass in dual fluidized bed gasifiers: a review. Renew Sust Energ Rev 98:64–78. https://doi.org/10.1016/j.rser.2018.09.010

35. Faust R, Berdugo Vilches T, Malmberg P, Seemann M, Knutsson P (2020) Comparison of ash layer formation mechanisms on si-containing bed material during dual fluidized bed gasification of woody biomass. Energy Fuels 34(7):8340–8352. https://doi.org/10.1021/acs.energyfuels.0c00509

36. Benedikt F (2020) Fuel flexible advanced dual fluidized bed steam gasification. Dissertation, TU Wien, Vienna. https://doi.org/10.34726/hss.2020.39988

37. Wolfesberger-Schwabl U (2013) Profiling tar behavior in dual fluidized bed biomass steam gasification, Dissertation, TU Wien, Vienna, https://permalink.catalogplus.tuwien.at/AC11451288. Accessed 23 May 2023

38. Bardolf R (2017) Optimierung eines Produktgaswäschers bei der Biomassedampfvergasung im Zweibettwirbelschichtverfahren. Dissertation, TU Wien, Vienna. https://doi.org/10.34726/hss.2017.36646

39. Kopyscinski J, Seemann MC, Moergeli R, Biollaz S, Schildhauer TJ (2013) Synthetic natural gas from wood: reactions of ethylene in fluidised bed methanation. Appl Catal A-Gen 462–463:150–156. https://doi.org/10.1016/j.apcata.2013.04.038

40. Loipersböck J, Lenzi M, Rauch R, Hofbauer H (2017) Hydrogen production from biomass: the behavior of impurities over a CO shift unit and a biodiesel scrubber used as a gas treatment stage. Korean J Chem Eng 34(8):2198–2203. https://doi.org/10.1007/s11814-017-0130-1

41. Seemann MC, Schildhauer TJ, Biollaz SMA (2010) Fluidized bed methanation of wood-derived producer gas for the production of synthetic natural gas. Ind Eng Chem Res 49(15):7034–7038. https://doi.org/10.1021/ie100510m

42. Witte J, Settino J, Biollaz SM, Schildhauer TJ (2018) Direct catalytic methanation of biogas – part I: new insights into biomethane production using rate-based modelling and detailed process analysis. Energy Conv Manag 171:750–768. https://doi.org/10.1016/j.enconman.2018.05.056

43. Rehling B (2012) Development of the 1MW Bio-SNG plant, evaluation on technological and economical aspects and upscaling considerations. Dissertation, TU Wien, Vienna. https://permalink.catalogplus.tuwien.at/AC07815367. Accessed 23 May 2023

44. Schweitzer D, Gredinger A, Schmid M, Waizmann G, Beirow M, Spörl R, Scheffknecht G (2018) Steam gasification of wood pellets, sewage sludge and manure: Gasification performance and concentration of impurities. Biomass Bioenerg 111:308–319. https://doi.org/10.1016/j.biombioe.2017.02.002